Highly Twisted Double-Helix Carbon Nanotube Yarns

Yuanyuan Shang,[†,‡] Yibin Li,[†,*] Xiaodong He,[†] Shanyi Du,[†] Luhui Zhang,[‡] Enzheng Shi,[‡] Shiting Wu,[‡] Zhen Li,[§] Peixu Li,[§] Jinquan Wei,[§] Kunlin Wang,[§] Hongwei Zhu,[§] Dehai Wu,[§] and Anyuan Cao[‡,*]

[†]National Key Laboratory of Science and Technology on Advanced Composites in Special Environments, Centre for Composite Materials and Structures, Harbin Institute of Technology, Harbin 150080, P. R. China, [‡]Department of Materials Science and Engineering, College of Engineering, Peking University, Beijing 100871, P. R. China, and [§]Key Laboratory for Advanced Materials Processing Technology and Department of Mechanical Engineering, Tsinghua University, Beijing 100084, P. R. China

ABSTRACT The strength and flexibility of carbon nanotubes (CNTs) allow them to be constructed into a variety of innovated architectures with fascinating properties. Here, we show that CNTs can be made into a highly twisted yarn-derived double-helix structure by a conventional twist-spinning process. The double-helix is a stable and hierarchical configuration consisting of two single-helical yarn segments, with controlled pitch and unique mechanical properties. While one of the yarn components breaks early under tension due to the highly twisted state, the second yarn produces much larger tensile strain and significantly prolongs the process until ultimate fracture. In addition, these elastic and conductive double-helix yarns show simultaneous and reversible resistance change in response to a wide range of input sources (mechanical, photo, and thermal) such as applied strains or stresses, light illumination, and environmental temperature. Our results indicate that it is possible to create higher-level, more complex architectures from CNT yarns and fabricate multifunctional nanomaterials with potential applications in many areas.

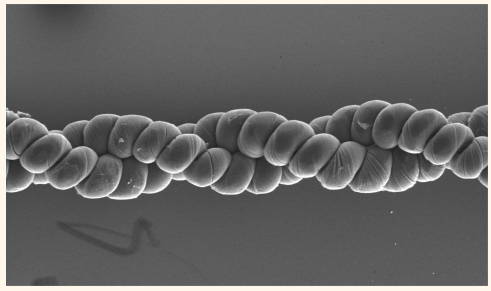

KEYWORDS: carbon nanotube · helical yarn · double-helix · hierarchical structure · nanomaterial sensor

Recently, carbon nanotube (CNT) and graphene yarns have stimulated tremendous interest owing to their potential applications in various areas such as sensors, actuators, electrodes for energy conversion and storage devices such as fiber-shaped solar cells and supercapacitors.[1−16] The close contact and strong interaction between twist-spun CNTs or self-assembled graphene sheets lead to enhanced mechanical strength and toughness, with good flexibility and a low material density close to aerogels. The porous yarn structure faciliates direct infiltration of polymers to make super-tough fibers and woven mats, or grafting of catalytic nanoparticles to improve the electrochemical reactivity and device efficiency in supercapacitors and solar cells.[9,14,17−20] Furthermore, appropriate structural modification, for example, by creating close-arranged helical loops in a overtwisted CNT yarn, results in superstretchable and spring-like ropes as reported in our previous work.[21] Extensive study has demonstrated that CNT and graphene yarns are promising materials to build novel structure, flexible and high performance electronic and electromechanical devices.

Thin and long CNT yarns, as a one-dimensional macroscopic assembly of nanotubes, also could serve as basic units to further construct higher-level architecture by controlled configuration of individual yarns. Previous study has demonstrated that the CNT yarns are both strong and flexible, which allow them to be coiled, twisted, braided, knitted, or knotted into diverse fascinating shapes. One structure of particular interest is the double-helix, which is widely observed in natural objects and also adopted by many biological species such as deoxyribonucleic acid (DNA) consisting of two spiral and spatially arranged strands. In this regard, a long and flexible CNT yarn may be considered as an ideal unit for building double-helices by hierarchical assembly. In fact, single twist-spun CNT yarns can be simply braided into two-ply and four-ply yarns to improve the loading capacity and toughness.[2] In addition, Q. Zhang, *et al.* have synthesized microscale CNT array double-helices on hydroxide flake substrates by

* Address correspondence to liyibin@hit.edu.cn, anyuan@pku.edu.cn.

Received for review November 8, 2012 and accepted December 30, 2012.

Published online December 30, 2012
10.1021/nn305209h

space-confined rotational growth.[22,23] Each strand consists of loose as-grown CNT bundles, and the electrical conductivity can be improved by solvent-induced densification of CNT strands although their mechanical properties remain unknown.

Here, we report a yarn-derived two-level hierarchical structure consisting of two highly twisted helical yarns in a configuration similar to a double-helix, and investigate the mechanical, electrical, and thermal properties of this multifunctional structure for a number of potential applications. In particular, we show a unique fracture mechanism involving the sequential breaking of yarn components that has not been found in separate or two-ply straight yarns. Compared to most of previous CNT yarns with a straight morphology, hierarchical helical yarns could bring material elasticity and other new mechanical properties, and extend the yarn applications to a wider area.

RESULTS AND DISCUSSION

We fabricated double-helix CNT yarns by continuously spinning a single-walled nanotube film through two overtwisting steps (see Experimental Methods), as illustrated in Figure 1a. The horizontally suspended CNT film was first spun into a straight yarn by an electric motor, then overtwisted into a single-helical yarn with a spiral shape, and further overtwisted into a double-helix made of two helical yarn segments. Detail structure characterization of single-walled nanotubes and the spinning process from a planar film into a helical yarn can be found in our previous publications.[21,24] Here, the formation of a double-helix was initiated by applying a small force in the middle section during spinning to trigger the rotation and mutual entanglement of two yarn segments from the left and right sides, and this process continued until the yarn ends led to a long uniform double-helix. When the nanotube film was spun from a planar film into a single-helical yarn, the yarn length was about $^1/_3$ of the film due to length reduction that accompanies the formation of helical loops. Upon formation of the double-helix, the overall sample length shrank by about $^1/_2$ again. Therefore, an as-synthesized 10 cm-long CNT film by chemical vapor deposition (CVD) resulted in a final double-helix length of 1−2 cm. Figure 1b illustrated a double-helix consisting of two single-helical yarns twisted mutually and in symmetry. It was actually a two-level hierarchical structure including the helical loop of each yarn and the spiral route in the overall double-helix. This structure was also different from braided CNT yarns made by twisting two straight (*versus* helical) yarns together in previous reports.[2]

Figure 1c showed the scanning electron microscopy (SEM) image of a spun double-helix CNT yarn which had a lateral size of ∼80 μm and length of several millimeters. Each of the two yarn segments making the double-helix had a diameter of ∼50 μm, and twisted with each other periodically at a pitch of ∼150 μm. The yarn segment itself was helical as well, with tiny loops close-arranged at a linear density of about 40 loops per millimeter. The tip (left end in Figure 1d) connecting two yarn segments was the middle point of the yarn where we applied a force in order to initiate the formation of the double-helix. Because the double-helix was formed by twisting two segments in the same yarn (film), a uniform starting film/yarn was critical for obtaining a straight, uniform, double-helix structure with controlled yarn diameter. A tight twisting process resulted in close contact between the loops in each helical yarn, indicating strong interaction at the yarn interface (Figure 1e,f). Narrow gaps between adjacent loops were sometimes observed due to the slight stretching along the yarn in such a highly twisted state, and traces of twisting could be distinguished on the surface of the helical loops (Figure 1g). Close view of the yarn surface revealed dense, parallel CNTs along the same direction in each loop (Figure 1h). The spinning and twisting processes could align CNTs from a random pristine film to aligned CNTs in the resulting straight and the double-helix yarn (Supporting Information Figure S1).

The double-helix was a more stable structure compared to a single helical yarn. During the spinning process, the overtwisting of the yarn caused internal strains and stress concentrations along random positions along the yarn length. Releasing one end of a helical yarn immediately caused a rebounding action in which the yarn shrank into an entangled aggregation. Among the aggregation we frequently found short-range double-helices with a similar morphology to that formed by controlled twisting (Figure 1i,j). These double-helices were produced by self-assembly when different yarn segments came into contact during rebounding, and therefore represented a more stable and favorable structure in the free state.

We performed mechanical tests on these double-helix CNT yarns to study their fracture mechanism and energy absorption during stretching. Tension tests on more than 10 samples with different yarn diameters revealed that the two helical yarns making the double-helix always broke one after the other, with a large difference in respective tensile strains. In other words, fracture of a double-helix occurred by two steps with one of the yarns breaking early and the other yarn breaking considerably later (Figure 2a). Tensile load−displacement curves revealed two linear loading stages connected in sequence before ultimate fracture (Figure 2b). The two samples shown here had an average yarn diameter of 70 and 100 μm, respectively, with similar mechanical response involving two loading stages. In the first stage, two yarns sustained the tensile force together until one of them broke and the force dropped suddenly to a lower level. Then the force increased linearly again by stretching the remaining yarn until the second yarn broke as well.

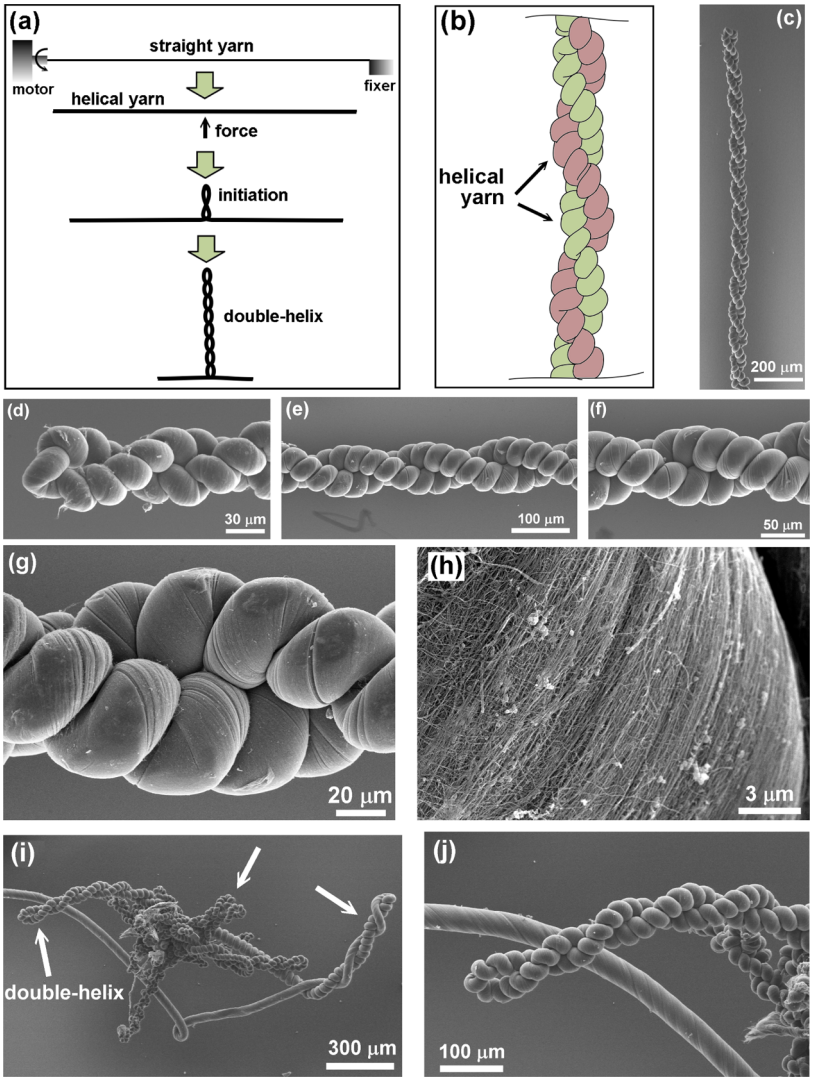

Figure 1. Fabrication and characterization of double-helix CNT yarns. (a) Illustration of a spinning process starting from a straight yarn, then a single-helical yarn by overtwisting, and then the formation of a double-helix by applying a small force in the middle part. (b) Illustration of the double-helix consisting of two single-helical yarns twisted together. (c) SEM image of a long and uniform double-helix. (d) Close view of the top end which is the initiation position for the double-helix. (e,f) SEM images of the middle section showing two helical yarns twisted tightly. (g) Enlarged view of the highly twisted double-helix. (h) High-magnification SEM image of the helical yarn surface showing numerous CNTs aligned along the twisting direction. (i) SEM image of an entanglement of double-helices (see arrows) formed by self-assembly. (j) Close view of a similar double-helix structure in the entanglement.

The force-strain curves were converted into stress−strain curves ($\sigma-\varepsilon$) based on the sum of cross-sectional areas of two yarns (for stage I) and the area of the remaining yarn for stage II (Figure 2c). There were two key features that can be derived from the stress−strain curves. In most cases the first yarn broke at a relatively small strain ($\varepsilon_1 < 100\%$) while the second yarn broke at a much larger strain ($\varepsilon_2 > 150\%$), resulting in a large difference in failure strains of the two yarns with $\varepsilon_2/\varepsilon_1$ ratios in the range of 1.7 to 3.2 (Figure 2d,e). Also, the second yarn broke at an increased stress than the first yarn, with σ_2/σ_1 ratios of 1.3−2.4. Measurement on approximately 11 double-helix yarns with yarn diameters of 55−110 μm revealed that the maximum relative stress and strain ratios were located in the diameter range of 70−90 μm (Figure 2e). The underlying mechanism was associated with the overtwisting of helical yarns which produced stress concentrations associated with curvature areas and structural defects. Therefore the first yarn broke early before it was stretched substantially and the helical loops remained there although they were more separated than in original form (Supporting Information, Figure S2). However, the breaking of the first yarn released the second yarn from the highly twisted state (a kind of stress relaxation), therefore the latter could sustain a much larger strain and stress. The stress relaxation could be observed by the sudden drop of stress upon the fracture of the first yarn followed by a quick rising of stress at the beginning of stage II (Figure 2c).

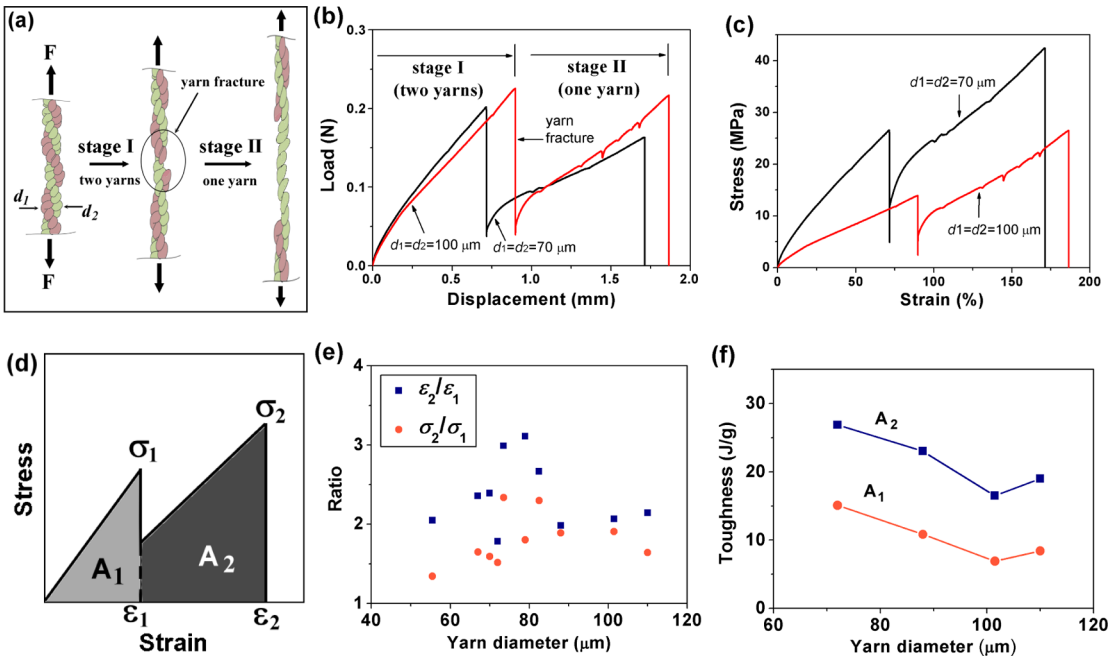

Figure 2. Mechanical testing on double-helix CNT yarns. (a) Illustration of the tensile testing process including two stages where two yarns sustain the force (*F*) together during stage I until one of the yarns fractures, and after that the remaining yarn is stretched during stage II until complete fracture. The diameters of the two yarns making the helix are d_1 and d_2, respectively. (b) Load−displacement curves of two double-helices with a yarn diameter of 70 and 100 μm, respectively. (c) Converted stress−strain curves by the load divided by the sum of cross-sectional area of the two yarns for stage I, and the load divided by the cross-sectional area of the remaining yarn for stage II. (d) Illustration of the tensile strengths (σ_1, σ_2), strains (ε_1, ε_2), and areas under each loading stage (A_1, A_2) for the two yarns, respectively. (e) Calculated σ_2/σ_1 and $\varepsilon_2/\varepsilon_1$ ratios for tested double-helices with different yarn diameters ranging from 50 to 110 μm. (f) Calculated areas (toughness) under the loading curves at stage I (A_1) and stage II (A_2), respectively.

SEM characterization of the tested samples after fracture also revealed that the second yarn was more stretched than the first one, with some loops straightened and even having disappeared (Supporting Information, Figure S2). The overall toughness could be calculated by the two areas enclosed under the two linear stages, and in general the area of stage II (A_2 = 17−26 J/g) was larger than that of stage I (A_1 = 7−15 J/g) for double-helices with different yarn diameters (Figure 2f). This was attributed to the increased strain and stress for the second yarn due to the stress relaxation by the breaking of the first yarn. Enhanced stress and toughness in the second yarn could be a useful property for structural applications where catastrophic failure need be avoided.

We have made a series of yarns with different pitches from 180 to 340 μm (Figure 3a). In our twisting process where the CNT yarns were twisted very tightly, the resulting double-helix pitch could be controlled and was determined by the individual yarn diameter, with an approximately linear relationship (slope = 4.5) (Figure 3b). Generally, the pitch value was about 4.5 times the yarn diameter. Mechanical tests showed that all samples fractured through two stages, with the first fracture occurring early for smaller pitches (Figure 3c). The results indicate that thinner yarns with smaller pitches made by our process tend to break at lower strains. Further, we twisted a straight and helical yarn into an asymmetric double-helix (Figure 3d), which also showed a two-stage fracture process including a first breaking of the straight yarn and a second breaking of the helical one (Figure 3e).

The sequential breaking mechanism was unique for the double-helix structure, and also found in a greater number of helical yarns twisted together (Supporting Information, Figure S3). In comparison, we twisted two straight yarns (spun from the same CNT film but without forming helical loops) into a similar double-helix structure, and measured its mechanical properties in tension under the same testing conditions (Supporting Information, Figure S4). The straight yarn-based double-helix showed much reduced tensile strains (ε < 40%), and the two component yarns broke either simultaneously or one after the other with a small difference in failure strains ($\Delta\varepsilon$ < 5%). This result indicated that the helical (*versus* straight) structure of individual yarns was important for the two-stage loading behavior observed in Figure 2. In addition, we also configured two helical yarns in parallel separately (not twisted together), and applied tensile force to fracture both yarns (Supporting Information, Figure S5). We observed that both yarns could sustain relatively high tensile strains (ε > 150%), but they broke one soon after the other at very close strains ($\Delta\varepsilon$ < 10%). In other words, after one yarn broke, the second one could not sustain any more strain and also broke very soon. This phenomenon was different than that of the double-helix yarns in which the second

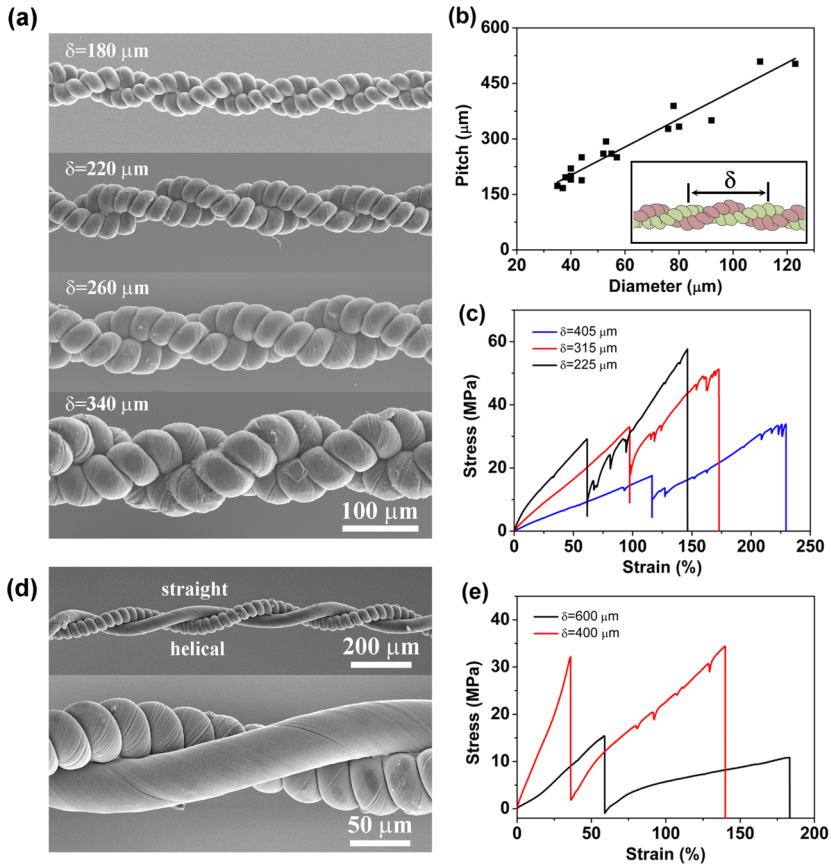

Figure 3. Control on the double-helix pitch and morphology. (a) SEM images of four double-helix yarns with different pitches from 180 to 340 μm. (b) Plots of measured pitch values (δ) *versus* yarn diameters. The inset illustrates the pitch of a double-helix. (c) Tensile stress−strain curves of three double-helix yarns with different pitches. (d) SEM images of an asymmetric double-helix consisting of a straight and helical yarn. (e) Tensile stress−strain curves of two asymmetric samples with different pitches.

yarn broke much later than the first one. The difference here was that parallel yarns did not have mutual interaction during deformation compared to a double-helix consisting of strongly twisted yarns.

Our multifunctional double-helix CNT yarns were elastic and electrically conductive, with clear response to various sources such as mechanical strain, incident light, and environmental temperature. Upon stretching, the yarn resistance changed simultaneously and linearly with increasing strain (Figure 4a). There was a step of sudden resistance increase when the first yarn broke, and after that the resistance increased again gradually until complete fracture. The helical yarns were also elastic within a certain strain range ($\varepsilon < 20\%$), and could recover to initial morphology without permanent deformation. Cyclic stress−strain curves measured on a double-helix yarn at a series of increasing maximum strains (ε = 5%, 10%, 15%, 20%, respectively) showed linear loading and unloading curves with a hysteresis loop (Figure 4b). This yarn showed full recovery after every cycle (stress remained above zero during unloading) and similar modulus during repeated loading, indicating high elasticity and structural stability in tension. Combining the electrical conductivity and mechanical elasticity could lead to potential applications such as strain or stress sensors. This property was demonstrated by recording the yarn resistance for many tensile cycles loaded to about 6.5 MPa every time, in which the resistance changed with stress consistently with a linear relationship (Figure 4c). The increase of resistance during stretching was likely due to the reduced contact area between the initially close-arranged helical loops.

The photo-response was tested by exposing a double-helix yarn to simulated solar illumination (AM 1.5, intensity = 80 mW/cm^2) and monitoring the current flow (I) through the yarn under a constant bias of 0.1 V applied at the two ends. The incident light was blocked by a shadow mask and arrived at the sample as pulses at an interval of about 3 s. Without illumination, the yarn maintained a constant current flow (stable resistance) in the dark over time ($\Delta I = 0$), whereas the current flow decreased instantaneously when receiving light pulses (Figure 4d). Although the percentage of current drop ($\Delta I/I$) was relatively small (~0.3%), the photo-response was stable and reversible for many cycles. We have studied related mechanism by changing the illumination range (visible and infrared) and applying or removing the bias. The double-helix showed current change in response to both simulated solar illumination (visible plus infrared) and

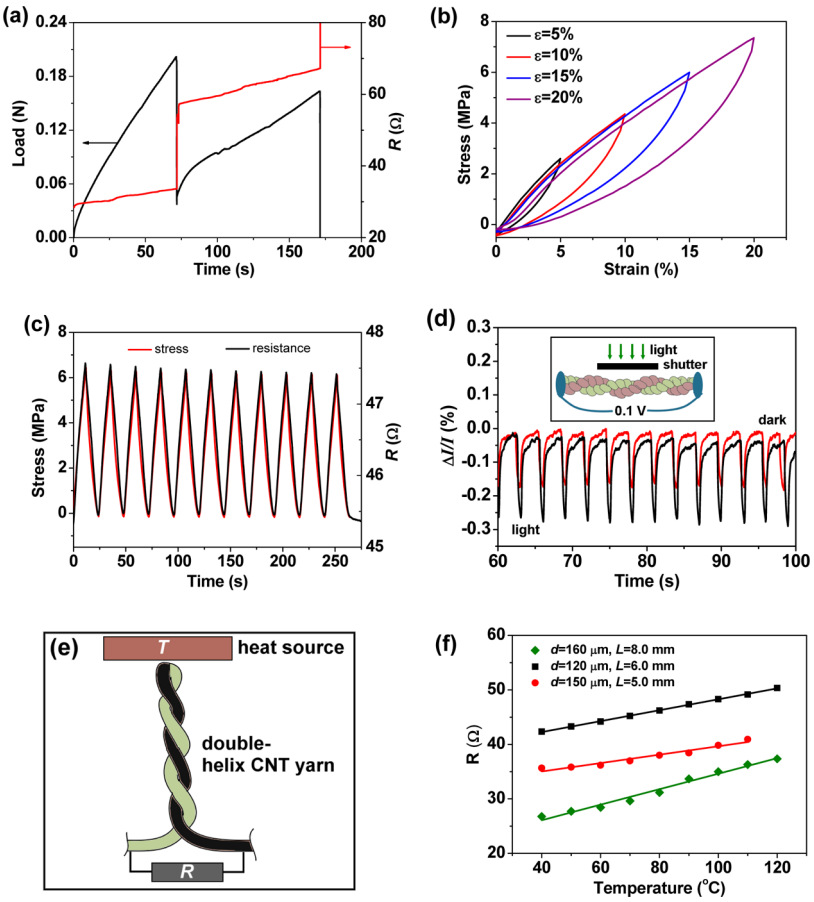

Figure 4. Properties and potential applications of CNT double-helix CNT yarns. (a) Tensile load-time curve of a double-helix CNT yarn with simultaneously recorded electrical resistance (*R*) accompanying the loading process. (b) Cyclic loading–unloading tensile tests of a double-helix yarn at predefined strains of 5% to 20% showing elastic behavior without residual deformation. (c) Recorded yarn resistance change during repeated stress cycles (up to 6.5 MPa). (d) Relative current change ($\Delta I/I$) in response to pulsed light illumination including visible and infrared range (black curve) and infrared (red curve, by blocking visible light). Inset shows the device setup with a shutter to control light pulses. (e) Illustration of a double-helix configured as a thermocouple to sense the temperature (*T*) increase in a heat source. (f) Resistance (*R*) values recorded in three different double-helix yarns (yarn diameter = *d*, total length between electrodes = *L*) during temperature increase from 40 to 120 °C, showing a linear *R*–*T* dependence.

infrared (visible light blocked by a conjugated polymer layer) under a bias of 0.1 V. After blocking visible light, the value of $\Delta I/I$ (induced mainly by infrared) decreased to about 50% ($\Delta I/I = 0.17\%$). When the bias was removed, the photocurrent generated in the yarn under light was very small (negligible) indicating that band gap light absorption by semiconducting CNTs was not a major factor. The current change as shown in Figure 4d was mainly due to the resistance increase in the yarn caused by the temperature change when the double-helix was irradiated.

The structure of our double-helix CNT yarns resembled a thermocouple including the node at the tip (initiation place for double helix) and the two yarns could be connected to the outside as electrodes. The yarn was made by metallic and semiconducting single-walled nanotubes that may display resistance change upon rising (or decreasing) temperature. We configured a double-helix temperature sensor with its tip in contact to the surface of a hot plate (as heat source), and its two yarns wired to a source meter to monitor the resistance (illustrated in Figure 4e). With steady temperature increasing from about 40 to 120 °C, the yarn resistance also increased at the same time with a close-to-linear relationship to temperature (Figure 4f). The resistance was measured through the entire yarn length (*L*) from one end to the other end of the double-helix. Three samples with different yarn diameters (120–160 μm) and lengths (5–8 mm) all displayed similar linear behavior in this temperature range, with calculated slopes in the range of 0.08–0.14 Ω/°C (Figure 4f). The results indicated that heating at the tip could effectively change the resistance through the double-helix, and unexpectedly, producing a linear *R*–*T* relationship. Upon cooling of the yarn, we still observed a linearly decrease of resistance however the tip contact to the heat source was not stable due to shrinkage and slight deformation of the double-helix during cooling. The double-helix structure was very convenient to be configured into a thermocouple for measuring the temperature of solid or liquid objects

with advantages such as lightweight and enhanced flexibility.

CONCLUSIONS

We adopted a simple and controllable method to produce double-helix CNT yarns with neat structure and distinct two-stage fracture behavior, which would be important for designing structures to prevent catastrophic failure. These double-helix structures demonstrated potential applications as strain sensors, photo detectors, and thermocouple-like devices. Given the mechanical strength, lightweight, and flexibility of CNT yarns, there is a great promise to fabricate hierarchical and more complex architectures and to explore their applications in many areas such as sensors, actuators, fiber-shape devices, and electrodes.

EXPERIMENTAL METHODS

Synthesis of CNT Films. Thin single-walled nanotubes films were synthesized by the CVD process with ferrocene (catalyst) and xylene (carbon source) as precursors. The ferrocene/xylene solution with a concentration of 5−10 μL/min was injected into the CVD furnace by a syringe pump. Reaction temperature was set at 1160 °C, and single-walled nanotubes grown in the vapor phase were carried out to the downstream zone by a gas mixture (Ar/H_2). Freestanding spiderweb-like CNT films were collected and used directly for spinning yarns.

Spinning of Double-Helix CNT Yarns. The spinning process included the following steps. First, a suspended CNT film with two ends fixed on an electric motor and a metal block fixer was spun into a straight yarn at a motor rotation speed of 100 rpm. Second, the straight yarn was further spun into a helical yarn by continued overtwisting at the same speed. Then, a small force was applied to the middle point of the helical yarn to initiate the formation of double-helix. The spinning was continued at a speed of about 50 rpm to produce a long double-helix CNT yarn. To spin an asymmetric double-helix (straight + helical), a straight yarn was twisted to form helical loops only in half part, and then the helical and remaining straight portions were twisted together into a double-helix.

Microstructure and Mechanical Measurement. The morphology and structure of the double-helix CNT yarns were characterized by SEM (Hitachi S4800). Mechanical tests were carried out in a single-column testing instrument (Instron 5843) equipped with a load cell of 10 N, and specially designed grips for holding small-size and fiber-shaped samples. The two ends of a double-helix CNT yarn were first fixed on a paper sheet with a cut window (0.5−2.5 cm long, depending on the length of tested yarn samples) by polyvinyl alcohol as adhesive paint. The paper was installed into the grips, with the fixed yarn aligned along the grip axis. Then the paper was cut from its two sides to free the double-helix CNT yarn. For tension tests, the upper grip was moved away at a constant speed of 1.0 mm/min. For cyclic tests, the strain rate was set to be 50% per minute for all the cycles. Two-ply straight yarns and parallel helical yarns were also fixed on a paper sheet and tested under the same condition.

Electrical, Light, and Temperature Response Measurements. To perform electrical measurements simultaneously with mechanical testing, the double-helix CNT yarn was connected to electrical wires by silver paste applied at its two ends. During cyclic tension tests, the current flow through the tested yarn section was also recorded by a source meter (Keithley 2635A) under a constant bias (0.1 V). The yarn resistance was calculated for the tested range of tensile strain during cycles.

The double-helix CNT yarn was exposed to simulated solar irradiation by a solar simulator (Newport Thermo Oriel 91195A) at air mass 1.5 and a light intensity of 80 mW/cm^2. The current flow through the yarn was recorded by connecting electrical wires to the two ends of the double-helix. A shutter was controlled manually to produce pulsed incident light to the sample at every 3 s. To blacken visible light, we spin-coated a thin layer (200 nm) of poly(3-hexylthiophene) (P3HT) on glass and placed it on top of the double-helix as a photomask.

To monitor the yarn resistance change during the environmental temperature change, the tip of a double-helix was placed in contact to the surface of a heating station (Wiggens WH220 Plus), which was heated at controlled rate to increase the surface temperature from 40 to 120 °C. The ends of the two helical yarns were connected to electrical wires to measure the resistance at an interval of 10 degrees.

Conflict of Interest: The authors declare no competing financial interest.

Acknowledgment. Y. Li and A. Cao gratefully acknowledge financial support from the National Science Foundation of China (NSFC) programs (Grant Nos. 11272109 and 51072005), and the fundamental research funds for the central universities (Grant No. HIT.BRETIII.201215).

Supporting Information Available: Additional figures and calculations as described in the text. This material is available free of charge *via* the Internet at http://pubs.acs.org.

REFERENCES AND NOTES

1. Li, Y.-L.; Kinloch, I. A.; Windle, A. H. Direct Spinning of Carbon Nanotube Fibers from Chemical Vapor Deposition Synthesis. *Science* **2004**, *304*, 276–278.
2. Zhang, M.; Atkinson, K. R.; Baughman, R. H. Multifunctional Carbon Nanotube Yarns by Downsizing an Ancient Technology. *Science* **2004**, *306*, 1358–1361.
3. Koziol, K.; Vilatela, J.; Moisala, A.; Motta, M.; Cunniff, P.; Sennett, M.; Windle, A. High-Performance Carbon Nanotube Fiber. *Science* **2007**, *318*, 1892–1895.
4. Zhang, X.; Jiang, K.; Teng, C.; Liu, P.; Zhang, L.; Kong, J.; Zhang, T.; Li, Q.; Fan, S. Spinning and Processing Continuous Yarns from 4-Inch Wafer Scale Super-Aligned Carbon Nanotube Arrays. *Adv. Mater.* **2006**, *18*, 1505–1510.
5. Xu, Z.; Gao, C. Graphene Chiral Liquid Crystals and Macroscopic Assembled Fibres. *Nat. Commun.* **2011**, *2*, 571.
6. Shin, M. K.; Lee, B.; Shin, H. K.; Lee, J. A.; Spinks, G. M.; Gambhir, S.; Wallace, G. G.; Kozlov, M. E.; Baughman, R. H.; Kim, S. J. Synergistic Toughening of Composite Fibres by Self-Alignment of Reduced Graphene Oxide and Carbon Nanotubes. *Nat. Commun.* **2012**, *3*, 650.
7. Dong, Z.; Jiang, C.; Cheng, H.; Zhao, Y.; Shi, G.; Jiang, L.; Qu, L. Facile Fabrication of Light, Flexible and Multifunctional Graphene Fibers. *Adv. Mater.* **2012**, *14*, 1856–1861.
8. Cong, H.-P.; Ren, X.-C.; Wang, P.; Yu, S.-H. Wet-Spinning Assembly of Continuous, Neat, and Macroscopic Graphene Fibers. *Sci. Rep.* **2012**, *2*, 613.
9. Dalton, A. B.; Collins, S.; Munoz, E.; Razal, J. M.; Ebron, V. H.; Ferraris, J. P.; Coleman, J. N.; Kim, B. G.; Baughman, R. H. Super-Tough Carbon-Nanotube Fibres. *Nature* **2003**, *423*, 703.
10. Zhao, H.; Zhang, Y.; Bradford, P. D.; Zhou, Q.; Jia, Q.; Yuan, F.-G.; Zhu, Y. Carbon Nanotube Yarn Strain Sensors. *Nanotechnology* **2010**, *21*, 305502.
11. Foroughi, J.; Spinks, G. M.; Wallace, G. G.; Oh, J.; Kozlov, M. E.; Fang, S. L.; Mirfakhrai, T.; Madden, J. D. W.; Shin, M. K.; Kim, S. J.; *et al.* Torsional Carbon Nanotube Artificial Muscles. *Science* **2011**, *334*, 494–497.
12. Guo, W.; Liu, C.; Zhao, F.; Sun, X.; Yang, Z.; Chen, T.; Chen, X.; Qiu, L.; Hu, X.; Peng, H. A Novel Electromechanical Actuation of Carbon Nanotube Fiber. *Adv. Mater.* **2012**, *24*, 5379–5384.
13. Chen, T.; Qiu, L.; Yang, Z.; Cai, Z.; Ren, J.; Li, H.; Lin, H.; Sun, X.; Peng, H. An Integrated Energy Wire for Both Photoelectric Conversion and Storage. *Angew. Chem., Int. Ed.* **2012**, *51*, 11977–11980.

14. Zhang, S.; Ji, C.; Bian, Z.; Yu, P.; Zhang, L.; Liu, D.; Shi, E.; Shang, Y.; Peng, H.; Cheng, Q.; *et al*. Porous, Platinum Nanoparticle-Adsorbed Carbon Nanotube Yarns for Efficient Fiber Solar Cells. *ACS Nano* **2012**, *8*, 7191–7198.
15. Chen, T.; Qiu, L.; Cai, Z.; Gong, F.; Yang, Z.; Wang, Z.; Peng, H. Intertwined Aligned Carbon Nanotube Fiber-Based Dye-Sensitized Solar Cells. *Nano Lett.* **2012**, *12*, 2568–2572.
16. González, C. J.; Martínez, C. E.; Lima, D. M.; Acik, M.; Rogers, M. D.; Sovich, J.; Haines, S. C.; Lepró, X.; Kozlov, M.; Zhakidov, A.; *et al*. Oriented Graphene Nanoribbon Yarn and Sheet from Aligned Multi-walled Carbon Nanotube Sheets. *Adv. Mater.* **2012**, *24*, 5695–5701.
17. Miaudet, P.; Badaire, S.; Maugey, M.; Derré, A.; Pichot, V.; Launois, P.; Poulin, P.; Zakri, C. Hot-Drawing of Single and Multiwall Carbon Nanotube Fibers for High Toughness and Alignment. *Nano Lett.* **2005**, *5*, 2212–2215.
18. Liu, K.; Sun, Y.; Lin, X.; Zhou, R.; Wang, J.; Fan, S.; Jiang, K. Scratch-Resistant, Highly Conductive, and High-Strength Carbon Nanotube-Based Composite Yarns. *ACS Nano* **2010**, *4*, 5827–5834.
19. Lima, M. D.; Fang, S.; Lepró, X.; Lewis, C.; Ovalle-Robles, R.; Carretero-González, J.; Castillo-Martínez, E.; Kozlov, M. E.; Oh, J.; Rawat, N.; *et al*. Biscrolling nanotube sheets and functional guests into yarns. *Science* **2011**, *331*, 51–55.
20. Lepró, X.; Ovalle-Robles, R.; Lima, M. D.; Elías, A. L.; Terrones, M.; Baughman, R. H. Catalytic Twist-Spun Yarns of Nitrogen-Doped Carbon Nanotubes. *Adv. Funct. Mater.* **2011**, *22*, 1069–1075.
21. Shang, Y.; He, X.; Li, Y.; Zhang, L.; Li, Z.; Ji, C.; Shi, E.; Li, P.; Zhu, K.; Peng, Q.; *et al*. Super-Stretchable Spring-Like Carbon Nanotube Ropes. *Adv. Mater.* **2012**, *24*, 2896–2900.
22. Zhang, Q.; Zhao, M.-Q.; Tang, D.-M.; Li, F.; Huang, J.-Q.; Liu, B.; Zhu, W.-C.; Zhang, Y.-H.; Wei, F. Carbon-Nanotube-Array Double Helices. *Angew. Chem., Int. Ed.* **2010**, *49*, 3642–3645.
23. Zhao, M.-Q.; Zhang, Q.; Tian, G.-L.; Huang, J.-Q.; Wei, F. Space Confinement and Rotation Stress Induced Self-Organization of Double-Helix Nanostructure: A Nanotube Twist with a Moving Catalyst Head. *ACS Nano* **2012**, *5*, 4520–4529.
24. Li, Z.; Jia, Y.; Wei, J.; Wang, K.; Shu, Q.; Gui, X.; Zhu, H.; Cao, A.; Wu, D. Large Area, Highly Transparent Carbon Nanotube Spiderwebs for Energy Harvesting. *J. Mater. Chem.* **2010**, *20*, 7236–7240.